The 5th European sCO2 Conference for Energy Systems
March 14-16, 2023, Prague, Czech Republic

2023-sCO2.eu-155

DESIGN AND COMPUTATIONAL ASSESSMENT OF A SUPERCRITICAL CO2 COMPRESSOR FOR WASTE HEAT RECOVERY APPLICATIONS

Alessandro Romei
Giacomo Persico*
Paolo Gaetani
Energy Department
Politecnico di Milano
Milan, Italy

Ernani Fulvio Bellobuono
Lorenzo Toni
Roberto Valente
Centrifugal compressors and expanders NPD
Baker-Hughes Nuovo Pignone
Florence, Italy

ABSTRACT

The development of novel technical solutions for the effective recovery of waste heat is crucial for making accessible the enormous amount of thermal energy released by industrial processes, thus supporting the EU energy strategy. To this end, the EU-H2020 project CO2OLHEAT aims at developing, and demonstrating in a real industrial environment, a novel sCO_2 power unit of 2-MW capacity recovering energy from flue gases at 400 °C. The thermo-economic optimization of the system and the complexity of its implementation led to select a simple recuperative cycle for the CO2OLHEAT unit, which features a relatively unconventional multi-shaft configuration where the sCO_2 compressor is driven by a dedicated radial expander, while the electrical power is generated via a separated axial turbine.

The present study focused on the design and computational assessment of the compressor for the CO2OLHEAT system. The thermodynamic optimization of the cycle led to an overall pressure ratio slightly above 2.5, delivered with a two-stage centrifugal compressor. As typically found in sCO_2 power systems, the thermodynamic state of the fluid at the machine intake (P = 85 bar; T = 32°C) is close to the critical point and to the saturation curve; therefore, the first stage of the machine demands a dedicated aero-thermodynamic design, which can account for the effects of non-ideal thermodynamics and of the potential onset of two-phase flows. The paper discusses the conceptual aero-mechanical design of the compressor and then focuses on its performance assessment over the full operating range via Computational Fluid Dynamics. Two alternative flow models are considered, the first one based on the experimentally-validated barotropic fluid representation, while the second one featuring a complete thermodynamic model which assumes homogeneous equilibrium between the phases. The approaches provide similar outcomes, showing that the compressor fulfills the system requirement and guarantees large rangeability.

INTRODUCTION

Energy-intensive industries across Europe release in the environment a large amount of hot flue gases, resulting in an enormous waste of heat which could, instead, be efficiently converted into useful mechanical or electrical energy. On the quantitative ground, considering recent statistics on waste heat not exploited [1], an average conversion efficiency of 25%, and an operating factor of 0.8, the conversion of 5% of the European waste heat would lead to more than 500 GWh of primary energy savings per year and, assuming 0.46 tCO2/MWh, it would avoid more than 100.000 tons of CO2 per year, with important economical relapses, further enhanced by the recent severe increase of fossil-fuel prices.

While for flue gas temperature below 300 °C and above 500 °C mature energy conversion technologies are available (Organic and Steam Rankine Cycles, respectively), such technologies exhibit techno-economical limitations for flue gas temperature within this range. For such conditions, which represent a large share of the overall available waste heat in Europe, alternative technologies are presently under study. Among them, closed Joule-Brayton thermodynamic cycles working with carbon dioxide in supercritical conditions (sCO_2) are particularly attractive due to the high efficiency of the system and the compactness of their components, which might foster fast response to transients and reduced footprint, which are crucial features for effective waste-heat recovery systems [2].

Even though advanced calculations were performed at both component ([3], [4], [5], [6], [7], [8], [9]) and system ([10], [11], [12], [13]) level, and the first experimental verification of components have given promising outcomes ([14], [15]), a proper demonstration of the overall system operation in the real environment is still needed. To this end, the EU-H2020 project CO2OLHEAT was launched in 2021, with the aim of developing a novel sCO_2 power system demonstration plant of 2-MW

* corresponding author: giacomo.persico@polimi.it

DOI: 10.17185/duepublico/77332

capacity, to be installed and operated in a real industrial environment, recovering waste heat from flue gases released at about 400 °C. By considering the flue gas conditions, as well as the required flexibility of operation, a simple recuperative sCO_2 cycle has been selected for the CO2OLHEAT system, with the sCO_2 compressor powered by a radial turboexpander and a subsequent axial turbine for electrical power generation.

The present study focuses on the design and the computational assessment of the sCO_2 compressor for the CO2OLHEAT power system. The thermodynamic optimization of the cycle led to an overall pressure ratio of 2.55, delivered by a two-stage centrifugal compressor. As typically found in such systems, at the machine intake the thermodynamic state of the fluid is close to the critical point and to the saturation curve (P = 85 bar; T = 32 °C); therefore, the first stage of the machine demands a proper aero-thermodynamic design, which must be capable to account for both the non-ideal thermodynamics of the fluid and the potential onset of phase change.

The design of the compressor was approached by leveraging the computational and modeling techniques developed in previous studies [9] and on the experimental survey recently carried out on a 5.4 MW sCO_2 prototype compressor [15], [16]. At first, a conceptual design of the meridional channel and of the blade was carried out, then the compressor aerodynamics was verified by applying Computational Fluid Dynamics (CFD) over the entire flow range of the machine. Two thermodynamic models of the fluid were considered: at first, the experimentally validated barotropic model was considered [17], which allows representing in a simplified way the non-ideal thermodynamics of the fluid and the onset of two-phase flows assuming homogeneous equilibrium between the phases; then, to enhance the reliability of the prediction, the compressor was also analyzed by applying a 'complete' homogeneous equilibrium model, which does not require the barotropic fluid assumption [18] and retains the actual thermodynamic complexity of the near-critical fluid.

The paper is structured as follows: at first the CO2OLHEAT system is presented and the compressor design process is described; then the compressor aerodynamics and performance are analyzed with the two computational models, to derive conclusions on the machine operation and on its modeling.

THE CO2OLHEAT POWER UNIT

The CO2OLHEAT power unit was conceived to recover waste heat from an existing cement plant, whose flue gases in nominal conditions are available at temperature of 400 °C and with a flow rate of 230000 Nm^3/h. The core of the system is a simple recuperated cycle without either recompression or recuperator bypass, due to the relatively low maximum temperature of the heat source and the high minimum stack temperature in order to avoid acid condenses (150 °C). As reported in Figure 1, in the overall system the power unit is complemented by a waste-heat recovery unit and by a water-based heat-rejection unit.

The thermodynamic optimization of the sCO_2 cycle led to set the compressor-intake thermodynamic conditions are set to 32 °C and 85 bar respectively, to properly exploit the high density of CO_2 in the proximity of the critical point. The compressor-outlet pressure is set to 216.9 bar, resulting from a trade-off between cycle performance, material selection, and cost. The resulting cycle pressure ratio is equal to 2.55, which is obtained by two centrifugal compressors in series; they are mechanically driven by two centripetal turbines in series, thus creating a compact turbo-expander unit. The maximum temperature of the cycle is set at 360 °C, namely 40 °C lower than the flue gas nominal temperature in order to limit the surface area of the primary heat exchanger. The expansion is completed by an axial turbine, which is responsible for the power output of the system.

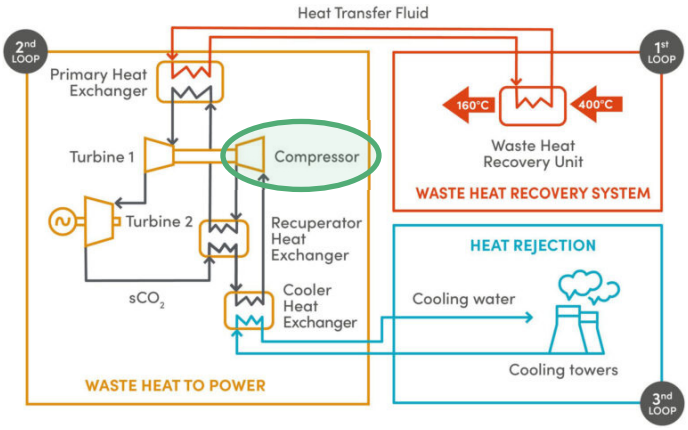

Figure 1: CO2OLHEAT system concept, with a focus on the compressor object of the study

The resulting net power output exceeds 2 MW, with a cycle efficiency of 23.17% referred to the inlet thermal power. Full details on the CO2OLEAT power system design and off-design operation can be found in [19].

COMPRESSOR DESIGN

The optimization of selected thermodynamic cycle requires the compressor to operate between 85 and 216.9 bar with inlet conditions very close to CO_2 critical point (32 °C, 670 kg/m3). Actual process conditions and the demo site available power lead to a compact machine size with an impeller diameter lower than 150 mm and a rotating speed close to 20000 RPM. In order to minimize the impact of internal leakages and to manage the residual axial thrust, an integrally geared configuration has been selected, which includes two shafts, one dedicated to the compression section and one to the expansion phase, as shown in Figure 2.

DOI: 10.17185/duepublico/77332

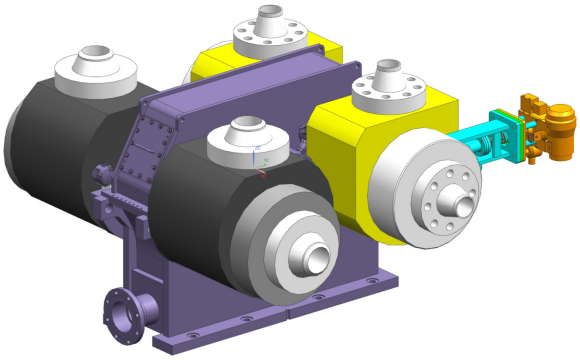

Figure 2: Turbo-expander compact system

The overall pressure ratio has been split into 2 centrifugal compressor stages in a back-to-back arrangement, as reported in Figure 3. The first compression phase is equipped with a movable axial inlet guide vane (IGV) to guarantee a fine-tuning of the suction operating condition, and to improve compressor flexibility in off-design conditions.

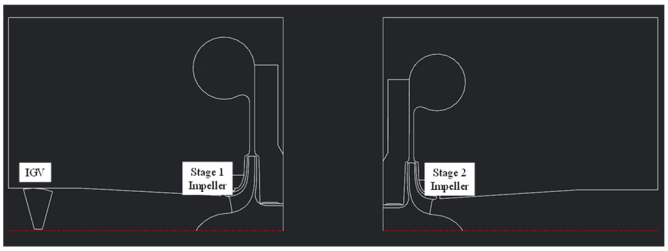

Figure 3: Back-to-back compressors configuration

The first impeller has a flow coefficient φ=0.0320, defined as $\boldsymbol{4Q_0/(\pi D_2^2 u_2)}$, and it features a dedicated design to cope with the CO_2 supercritical characteristics. CO_2 thermodynamic conditions at the inlet flange, in fact, are slightly above the critical ones, with small margins with respect to the saturation lines. Moreover, the unavoidable pressure drop which occurs from the inlet flange to the first impeller suction section further decreases this margin.

For these reasons, phase change could occur in suction regions inside the machine, around the IGV blades and inside the first impeller. Specifically, the suction side of the blade, in the proximity of the leading edge, typically shows the lowest static pressure level and, potentially, a two-phase flow could onset in the rotor channel. Where static pressure decreases below the saturation one, an abrupt change occurs in many thermodynamic quantities, the most important of which are density and speed of sound. As described in the following paragraph, the design of this machine requires an approach leveraged on proper numerical modeling, able to deal with both strong non-ideal gas behavior and the effect of potential phase change.

Impeller design, therefore, has been focused on avoiding phase change or limiting it to very small regions with also actual CO_2 real gas characteristics considered. To this end, in the stage conceptual design, the following features have been selected: at first, an impeller equipped with splitter blades to decrease the blockage at the inlet and mitigate the risk of anticipated chocking; secondly, an appropriate definition of the impeller cross-section evolution to take into account the low compressibility of sCO_2.

NUMERICAL METHODS

The computational flow model is based on the pressure-based Ansys Fluent finite-volume flow solver. In this work, we compare two computational frameworks to deal with non-ideal compressible two-phase flows of CO_2, named *homogeneous equilibrium model* (HEM) and *barotropic mode*, respectively. Both models describe the two-phase flow in terms of mixture properties, hence single-phase governing equations are recovered and expressed in terms of proper averaged properties. The turbulence effects are included with the $k-\omega$ SST model [20], adding a rotation-curvature correction to the production terms of k and ω [21]. Whenever walls are modeled as smooth, the turbulence equations are resolved at the wall having wall-adjacent cells in the viscous sublayer, i.e. $y^+ < 3$. Otherwise, wall functions are employed to account for roughness effects.

The HEM features an enthalpy-based energy equation in place of the standard energy equation based on the total enthalpy. In this way, thermodynamic equilibrium properties for the two-phase flow can be easily invoked by using pressure and static enthalpy as independent state variables. To speed up the calculation, a look-up-table (LUT) approach is implemented to call thermodynamic properties within flow solver iterations. The LUT boundaries are set to avoid extrapolated values in the solution, and they are $P \in [20, 300]\ bar$ and $h \in [151, 588]\ kJ/kg$, with $h_{ref} = 200\ kJ/kg$ at $T = 273.15\ K$ and saturated liquid condition. 1201×1201 grid points are identified by uniform steps in pressure (0.233 bar) and specific enthalpy (0.364 kJ/kg). The detailed formulation of the flow model, its validation against experimental data, and the appropriateness of the LUT discretization are discussed in [18].

On top of the HEM assumptions, the barotropic model introduces a simplification in the thermodynamic treatment. Thermodynamic and transport properties are computed as a function of the local pressure and the upstream entropy, hence neglecting the thermal and volumetric contributions due to loss generation. Thanks to the barotropic assumption the mass and momentum equations are decoupled from the energy one, which does not need to be explicitly resolved. A similar LUT approach is implemented for the barotropic model: thermophysical properties are tabulated as a function of pressure at the upstream entropy, using for pressure the same boundaries and discretization step reported for the HEM. Such a model, though thermodynamically simplified, is deemed to be particularly relevant for turbocompressor applications, since heat transfer is usually negligible in such components and computational efficiency is crucial for their aerodynamic design and optimization. The barotropic model was first proposed for application to sCO_2 compressors by the same authors in [9], and

DOI: 10.17185/duepublico/77332

it was subsequentially validated against experimental data of a MW-scale sCO_2 centrifugal compressor prototype in [15].

The system of equations (continuity, momentum, energy, and turbulence) is solved in the following way: continuity and momentum are solved in a coupled fashion, then the two turbulence equations and, if needed, the enthalpy-based energy equation. After this step, thermo-physical properties are updated, and the procedure is iterated until achieving numerical and physical convergence. Advective terms of continuity, momentum, and enthalpy-based energy equation are discretized with the QUICK scheme. A cell-to-cell flux limiter is applied to reduce spurious oscillations near discontinuities. Advective terms of turbulence equations are discretized with a linear upwind scheme. All diffusive terms are discretized with a second-order central differencing scheme. The gradients are computed with the least squares cell-based method. A second-order accurate method is selected to interpolate the pressure from cell centers to cell faces.

The computational grid is composed of hexahedral elements and was generated with AutoGrid™. The computational domain includes the main and splitter blade, with fillet radii, and the vaneless diffuser. A single-blade passage is modelled, by exploiting periodic boundary conditions. As the aim is to investigate the internal flow aerodynamics, the inlet guide vanes, as well as the leaks in the seals and the related secondary flows, were not the object of the CFD simulation. After a preliminary grid-dependence analysis, a mesh composed of about 3 million cells was adopted.

Calculations were performed by assigning the total state at the inlet section. The flow rate was imposed at the outflow, except close to choked-flow conditions, for which an average static pressure was assigned at the outlet. No-slip boundary conditions were imposed on the solid walls. As the flow domain is rotating with the impeller, a counter-rotating velocity was assigned at the endwalls of the vaneless diffuser.

COMPRESSOR PERFORMANCE

The computational flow models described in the previous section were applied to investigate the aerodynamic performance of the first stage of the CO2OLHEAT compressor, namely the one most affected by the near-critical fluid state and which demanded a tailored design. Since the predictions obtained by applying the barotropic model were experimentally validated in previous studies [15], this model was considered for a first assessment of the compressor performance. In this first analysis, conventional smooth walls are considered. Figure 4 reports two operational curves of the machine, related to the pressure ratio (top) and total-total efficiency (bottom) for the nominal angular speed and meridional flow at the intake (corresponding to IGV stagger position equal to 0°). The curves are scaled with respect to the values obtained for the nominal condition, for confidentiality reasons.

Curves cover a wide range of flow conditions, from 75% to 145% of the design flow rate. On the curves, the chocking limit (labelled as “C”) and the left one (labelled as “L”) are reported.

The left limit was, in fact, set *a priori*, since no expected plant operating condition should require flow coefficients below that value (also in consideration of the availability of IGVs). However, it is important to remark that the simulations for the lowest flow rate condition did not exhibit any trace of computational instabilities which normally arise approaching aerodynamic stall, thus suggesting that the actual left limit of the machine may be extended below the 75%.

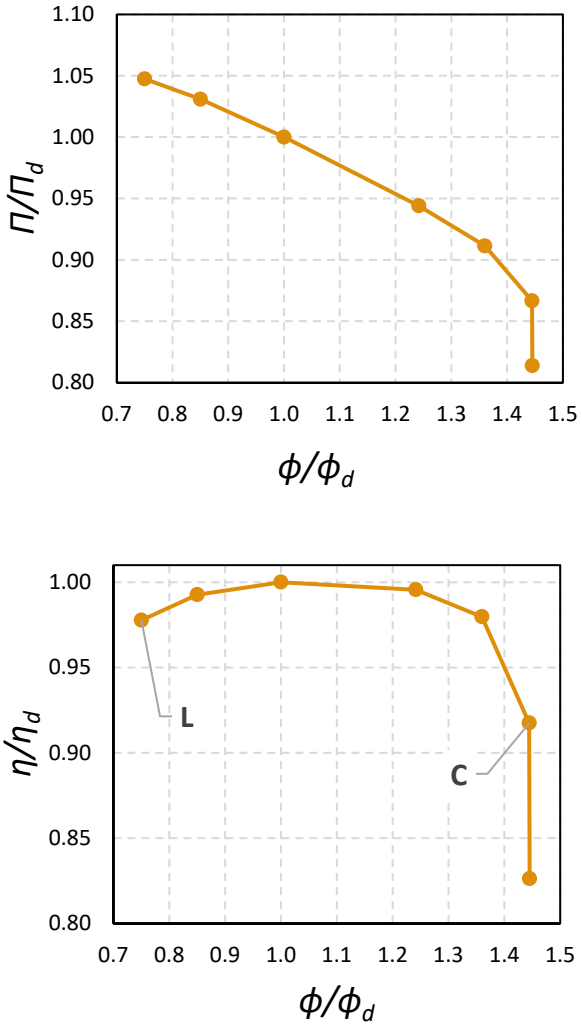

Figure 4: Operational curves of the first stage of the compressor simulated with the barotropic model and smooth walls. Top: pressure ratio; bottom: total-total efficiency

As further proof of that, the left frame of Figure 5 shows the distribution of relative Mach number in the midspan section for the lowest flow rate considered. The figure indicates a low level of compressibility, as the relative Mach number remains below 0.3 in almost the whole blade midspan section; local accelerations appear on the suction side of the blades, as a

DOI: 10.17185/duepublico/77332

consequence of the positive incidence, but no traces of local separation appear, thus excluding any risk of blade stall. Similar considerations apply to the flow in the endwall regions, in particular close to the blade tip, where the highest relative Mach number and incidence are found. In the context of sCO_2 compressors, due to the near-critical intake state, the aforementioned local accelerations may lead to the onset of phase change, which occurs as cavitation for the present case [3], [22], [9]. Due to the abrupt drop of speed of sound in the two-phase region [23], the cavitation is normally accompanied by an abrupt rise in Mach number. Since such a feature clearly does not appear in the present case, one can conclude that the combination of the selected thermodynamic state and of the compressor intake design prevents from the onset cavitation, at least for low flow rate conditions.

An analysis of the flow, density, and pressure fields in the nominal condition, not reported for sake of brevity, confirms that the risk of phase change at the compressor intake is almost completely avoided thanks to the tailored rotor design.

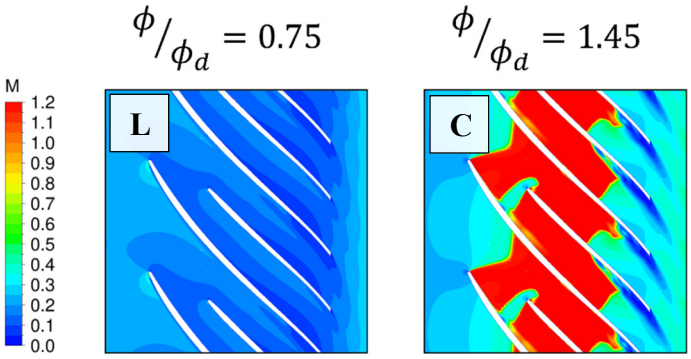

Figure 5: Mach number distributions at midspan for 75% (left) and 145% (right) of the nominal flow rate.

The situation is completely different for the conditions close to right limit. The curves clearly show the onset of choking for a flow rate equal to 145% of the design, verified by running multiple CFD simulations for different pressure ratios. Even though occurring at high flow rate, the chocking is anticipated with respect to the value expected by neglecting the onset two-phase flows; this phenomenon was clearly shown in a previous study, where a CO_2 compressor was operated in conditions near and far from the critical point [24]. The right frame of Figure 5, showing the Mach number distribution at midspan for the right limit condition, shows that upstream of the blades the Mach number remains below 0.5; however, as the flow enters within the bladed channel, the combination of blade thickness, blade aerodynamics, and negative incidence promotes a static pressure drop sufficiently large to trigger phase change; this, in turn, implies an abrupt rise of relative Mach number, causing the onset of choking. The value of the chocking flow rate, which in principle might depend on the degree of chemical and thermal equilibrium established between the phases of mixture, was found to be properly captured by models based on the homogeneous equilibrium assumption, such as the present barotropic one, by virtue of an experimental validation study made on a MW-scale sCO_2 compressor [15].

In light of the present analysis, the first CO2OLHEAT compressor is capable to provide the expected performance in a very large range of operation, greatly limiting the most severe effects of two-phase flows to very high flow rate conditions, not even expected in the off-design operation of the system.

MODEL COMPARISON

The CFD model based on the barotropic fluid assumption was experimentally validated and features a computationally-effective mathematical formulation. However, in an effort of improving the generality of sCO_2 compressor simulation tools, its verification against more complex models is relevant, at least to evaluate its range of validity and limitations. To this end, the aerodynamics of the first CO2OLHEAT compressor was simulated with a complete CFD-HEM, namely a computational model capable of simulating the dynamics of two-phase mixtures without resorting to the barotropic assumption. In this way, the thermal and volumetric effects of entropy generation across the compressor are taken into account and, hence, a correction on the meridional flow component might occur, with potential implications on the work exchange, pressure rise, and compressor efficiency. When constructing this 'reference' simulation tool, we still focused on a model that treats the two-phase flow assuming homogeneous equilibrium between the phases. This is motivated by the experimental validations available in literature for flashing flows in sCO_2 nozzles [17], ejectors [25] and sCO_2 compressors [15], which all agree in recognizing a good capability of the HEM in reproducing the phase change processes evolving from near-critical states. For this reason, the generalization of the barotropic model was focused on the single-phase thermodynamics rather than on the multi-phase model.

Figure 6 reports the operational curves, in terms of pressure ratio and efficiency as simulated by both the barotropic model and the HEM. The curves exhibit a noteworthy agreement, both qualitative and quantitative, suggesting that the thermal effects play a negligible role in the compressor performance. In an effort of explaining the obtained results, Figure 7 reports the streamwise evolution of density and meridional velocity component along the compressor in the nominal operation for both the computational models. The density distribution exhibits a slight reduction upstream of the main-blade leading edge (placed at a streamwise coordinate equal to 0.23), followed by a regular increasing trend, which terminates with a density increase of about 10% of the intake value (which indicates the low compressibility of the fluid in the present condition). As already stated, the physical effect not captured by the barotropic model is the volumetric implication of dissipation, which increases the thermal energy of the fluid as entropy generates along the irreversible compression process.

DOI: 10.17185/duepublico/77332

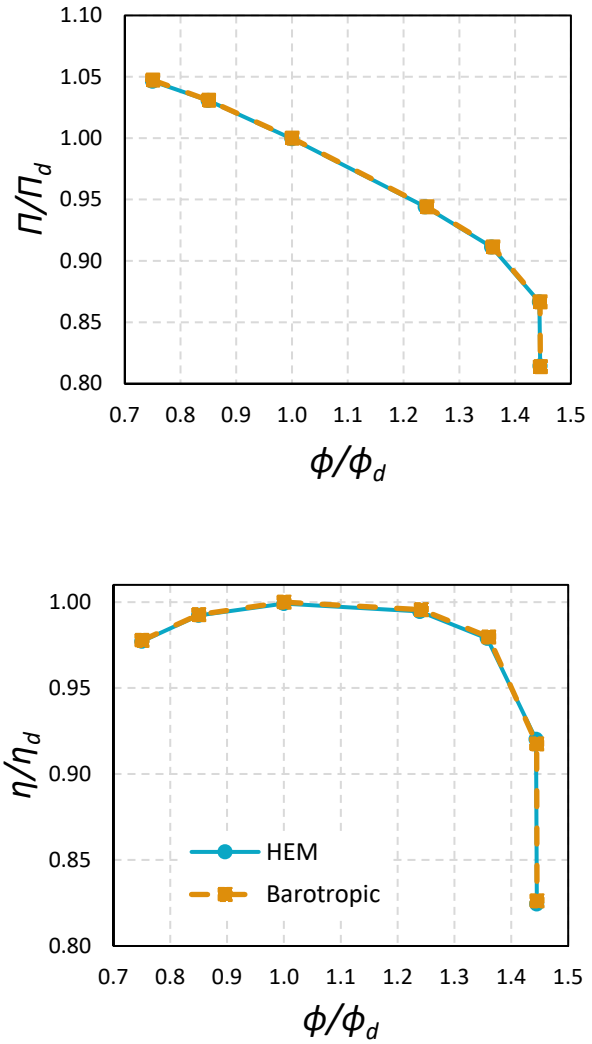

Figure 6: Comparison between operational curves of the first stage of the compressor simulated with the barotropic model and the HEM, for smooth walls.

Figure 7 actually shows a deviation between barotropic and HEM predictions as the compression proceeds along the machine with, as expected, a lower density computed by the HEM. Such differences are completely negligible along the impeller (the trailing edge of the blades is placed at a streamwise coordinate of 0.62) while they become visible in the vaneless diffuser section (due to the entropy generated downstream of the impeller). The maximum difference, however, is of the order of 0.2% of the actual density value, or 2% of the (already low) overall change in density across the machine.

The change in density, though small, might have an impact on the flow configuration and in the velocity triangles, as it alters the meridional flow component. For this reason, Figure 7 also reports the streamwise distribution of the meridional flow velocity for barotropic and HEM predictions. The distribution shows an increase in meridional velocity within the impeller, with local disturbances in correspondence of the leading and trailing edge of the blades. The diagram indicates that the impact of the barotropic assumption is everywhere negligible, so the cinematics of the machine is properly estimated by both the models.

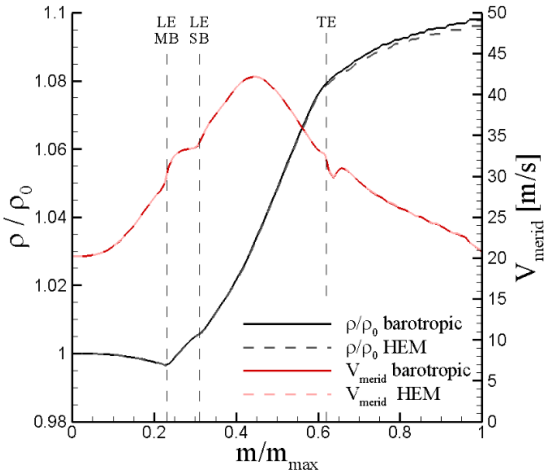

Figure 7: Streamwise evolution of density and meridional flow velocity along the meridional coordinate in nominal condition (LE-MB : leading edge main blades, LE_SB : leading edge splitter blades; TE: blades trailing edge).

Figure 8 reports the same quantities as Figure 7 for the two limit conditions of operation of the compressor, identified in Figure 4. The same considerations made for the nominal condition apply to the low flow rate one, while a different flow configuration emerges at high flow rate, which is characterized by cavitation-induced choking. In this latter case, the density of the fluid undergoes a severe drop in the proximity of the main-blade leading edge and further reduces in correspondence to the leading edge of the splitter blade; the density finally reaches its minimum value in the central region of the channel, where the meridional velocity exhibits its peak value, and the two-phase mixture occupies the whole channel. Then, the density progressively rises and the fluid revers to single phase in the rear part of the impeller (from ~0.52 streamwise coordinate onwards). In the central part of the channel, where the largest oscillations take place, the models exhibit slight local differences in density, which however disappear in the rear part of the impeller; as already observed in the other conditions, a residual marginal difference in density remains at the stage exit, of about 0.6% of the local density value, or 1.6% of the density variation along the impeller. In terms of meridional flow velocity, minor variations appear also in this case, even in the two-phase region in the center of the channel.

This analysis explains why the barotropic flow model is able to reproduce the complexity of the sCO_2 compressor aero-thermodynamics, at least for the thermodynamic condition of interest for this study. However, operating sCO_2 in the present thermodynamic region is advantageous for sCO_2 power systems,

DOI: 10.17185/duepublico/77332

so the validity of the present modeling is deemed relevant for the sCO_2 technology and not only for this specific case.

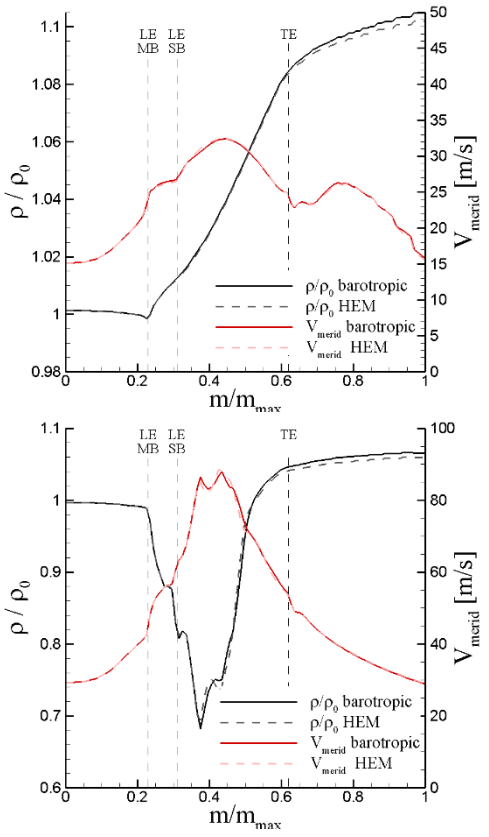

Figure 8: Streamwise evolution of density and meridional flow velocity along the meridional coordinate for 75% (top) and 145% (bottom) of the nominal flow rate.

IMPACT OF WALL ROUGHNESS

The power capacity of waste heat recovery systems is relatively low with respect to conventional power systems, especially in the present demonstration plant. This feature, combined with the inherent compactness of sCO_2 machines, makes size-effects particularly relevant for the CO2OLHEAT compressors. In an effort of investigating the aerodynamic impact of small size, a computational evaluation of the wall roughness was performed, using the complete HEM model and simulating the entire range of machine operation. An equivalent sand grain roughness k_s equal to 5 μm was selected, representative of a standard manufacturing technology, though not indicative of the manufacturer's capabilities. Nonetheless, for this fluid in the thermodynamic conditions of interest the thickness of the viscous sublayer is estimated to be of the order of 10^{-2} μm, thus one might expect that such a value of surface roughness will alter the development of the boundary layer and the associated loss generation.

Figure 9 compares the curves of total-total pressure ratio and efficiency of the first stage of the CO2OLHEAT compressor showing important quantitative effects. In the nominal flow rate conditions, the roughness reduces by 1% the pressure ratio and 3% the efficiency. These differences are maintained fairly constant along the whole operating range (the lower difference appearing at the choking is, in fact, an artificial effect of the nearly vertical shape of the curve in this region, which greatly complicates the comparison between different conditions). Moreover, the roughness does not influence the left limit, where, again, no traces of stall onset appeared in the simulations, and especially at choking, which is reached for the same flow rate as the smooth-wall calculation.

These results confirm the significant quantitative role of wall roughness in terms of compressor performance, suggesting care in the selection of the manufacturing process, but they also indicate a limited impact of roughness on compressor rangeability.

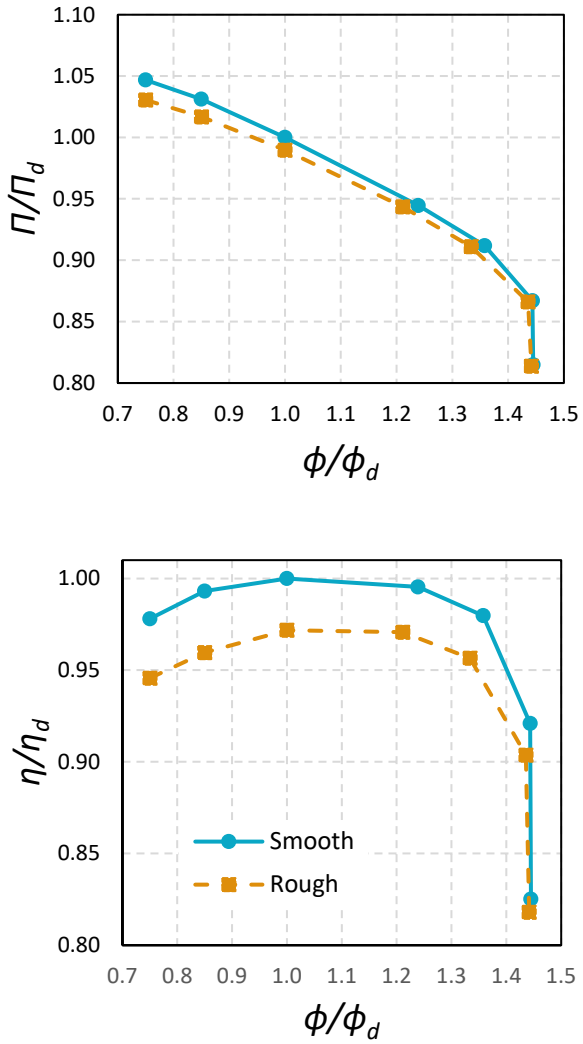

Figure 9: Effect of the wall roughness on the operational curves of the first stage of the compressor simulated with the HEM.

DOI: 10.17185/duepublico/77332

CONCLUSION

This paper has presented the design and the computational analysis of the near-critical sCO_2 compressor of the CO2OLHEAT waste heat recovery system. The machine, composed by two back-to-back compressor stages, features an integrated architecture and a non-conventional design approach for the first impeller, due to the thermodynamic complexity associated to the working fluid, which is operated close to the thermodynamic critical point.

The aerodynamics of the first stage of the compressor was analyzed with Computational Fluid Dynamics, applying both an experimentally-validated solver based on the barotropic fluid model and an alternative solver based on a more complete thermodynamic model. Both the solvers are capable of simulating non-ideal two-phase flows of sCO_2, under the assumption of homogeneous equilibrium between the phases. The two models have been shown to provide very similar results, with minor quantitative differences in local regions of the flow, negligible in terms of fluid kinematics.

The first stage of the compressor was analyzed in multiple operating conditions, so to characterize the entire range of machine operation, and it was shown to guarantee rangeability in the range 75% - 145% of the nominal flow rate. The left limit is, in fact, set a priory and does not exhibit any stall onset; the right limit is caused by the onset of choking, due to the phase-change process. A detailed investigation of the compressor aerodynamics reveals that, thanks to the dedicated machine design of the intake region, two-phase flows are negligible for the left side of the curve, and become significant only above nominal flow rate.

Finally, the size-effect associated with the wall roughness was investigated, showing a relatively significant influence on the compressor performance (up to 3% of efficiency, for a sand grain roughness of 5 microns, fairly constant along the compressor curve), but a negligible impact on the compressor rangeability.

NOMENCLATURE

Π	total-total pressure ratio
η	total-total efficiency
ϕ	flow coefficient
M	Mach number
ρ	density [kg/m^3]
V	velocity [m/s]
m	streamwise coordinate

Subscripts

0	intake thermodynamic state
d	nominal condition
max	maximum value
merid	meridional component

ACKNOWLEDGEMENTS

The CO2OLHEAT project has received funding from the European Union's Horizon 2020 research and innovation programme under grant agreement N° 101022831.

REFERENCES

[1] O. Reimann, "CEWEP Energy Report III (Status 2007-2010)," Confederation of European Water-to-Energy Plants, www.cewep.eu, 2012.

[2] M. Marchionni, G. Bianchi and S. Tassou, "Review of supercritical carbon dioxide (sCO2) technologies for high-grade waste heat to power conversion," *SN Applied Sciences,* vol. 2, no. 611, 2020.

[3] R. Pecnik, E. Rinaldi and P. Colonna, "Computational fluid dynamics of a radial compressor operating with supercritical CO2," *Journal of Engineering for Gas Turbines and Power,* vol. 134, no. 12, 2012.

[4] N. D. Baltadjiev, C. Lettieri and Z. S. Spakovszky, "An investigation of real gas effects in supercritical CO2 centrifugal compressors," *Journal of Turbomachinery,* vol. 137, 2015.

[5] R. Pelton, T. Allison, S. Jung and N. Smith, "Design of a Wide-Range Centrifugal Compressor Stage for Supercritical CO2 Power Cycles," in *ASME Turbo xpo 2017*, Charlotte, NC, USA, 2017.

[6] A. Hacks, S. Schuster, H. J. Dohmen, F. K. Benra and D. Brillert, "Turbomachine Design for Supercritical Carbon Dioxide Within the sCO2-HeRo.eu Project," *Journal of Engineering for Gas Turbines and Power,* vol. 140, 2018.

[7] M. Marchionni, L. Chai, G. Bianchi and S. Tassou, "Numerical modelling and transient analysis of a printed circuit heat exchanger used as recuperator for supercritical CO2 heat to power conversion systems," *Applied Thermal Engineering,* vol. 161, no. 114190, 2019.

[8] A. Hosangadi, Z. Liu, T. Weathers, V. Ahuja and J. Busby, "Modeling multiphase effects in CO2 compressors at subcritical inlet conditions," *Journal of Engineering for Gas Turbines and Power,* vol. 141, no. 8, 2019.

[9] G. Persico, P. Gaetani, A. Romei, L. Toni, E. Bellobuono and R. Valente, "Implications of phase change on the aerodynamics of centrifugal compressors for supercritical carbon dioxide applications," *Journal of Engineering for Gas Turbines and Power,* vol. 143, no. 4, 2021.

[10] V. Dostal, A Supercritical Carbon Dioxide Cycle for Next Generation, Ph.D. thesis, Massachusetts Institute of Technology, 2004.

[11] S. A. Wright, R. F. Radel, M. E. Vernon, G. E. Rochau and P. S. Pickard, *Operation and Analysis of a Supercritical CO2 Brayton Cycle,* Sandia Report SAND2010-0171, 2010.

[12] A. Romei, P. Gaetani, A. Giostri and G. Persico, "The role of turbomachinery performance in the optimization of supercritical carbon dioxide power systems," *Journal of Turbomachinery,* vol. 142, no. 7, p. 071001, 2020.

[13] D. Alfani, M. Binotti, E. Macchi, P. Silva and M. Astolfi, "sCO2 Power Plants for Waste Heat Recovery: Design

DOI: 10.17185/duepublico/77332

Optimization and Part-Load Operation Strategies," *Applied Thermal Engineering,* vol. 195, 2021.

[14] J. Mortzheim, D. Hofer, S. Piebe, A. McClung, J. J. Moore and S. Cich, "Challenges With Measuring Supercritical CO2 Compressor Perform-ance When Approaching the Liquid-Vapor Dome," in *ASME Turbo Expo 2021*, 2021.

[15] L. Toni, E. Bellobuono, R. Valente, A. Romei, P. Gaetani and G. Persico, "Computational and Experimental Assessment of a MW-Scale Supercritical CO2 Compressor Operating in Multiple Near-Critical Conditions," *Journal of Engineering for Gas Turbines and Power,* vol. 144, no. 10, 2022.

[16] M. Bigi, V. Bisio, S. Evangelisti, M. Giancotti, A. Milani and T. Pellegrini, "Design and Operability Challenges for Supercritical CO2 Plants: The sCO2-Flex Centrifugal Compressor Test Experience," in *ASME Turbo Expo 2022*, 2022.

[17] A. Romei and G. Persico, "Computational fluid-dynamic modelling of two-phase compressible flows of carbon dioxide in supercritical conditions," *Applied Thermal Engineering,* 2021.

[18] A. Romei, P. Gaetani and G. Persico, "Computational fluid-dynamic investigation of a centrifugal compressor with inlet guide vanes for supercritical carbon dioxide power systems," *Energy,* 2022.

[19] D. Alfani, M. Asolfi, M. Binotti, P. Silva and G. Persico, "Part load analysis of a constant inventory supercritical co2 power plant for waste heat recovery in cement industry," in *The 5th European sCO2 Conference for Energy Systems*, 2023.

[20] F. R. Menter, "Two-Equation Eddy-Viscosity Turbulence Models for Engineering Applications," *AIAA Journal,* vol. 32, no. 8, pp. 1598-1605, 1994.

[21] P. E. Smirnov and F. R. Menter, "Sensitization of the SST Turbulence Model to Rotation and Curvature by Applying the Spalart–Shur Correction Term," *Journal of Turbomachinery,* vol. 131, no. 4, p. 041010, 2009.

[22] S. Saxena, R. Mallina, F. Moraga and D. Hofer, "Numerical Approach for Real Gas Simulations: Part II – Flow Simulation for Supercritical CO2 Cen-trifugal Compressor," in *ASME Turbo Expo 2017*, 2017.

[23] C. E. Brennen, Fundamentals of Multiphase Flows, Cambridge University Press, 2005.

[24] L. Toni, E. F. Bellobuono, R. Valente and A. R. P. G. G Persico, "Experimental and Numerical Performance Survey of a MW-Scale Supercritical CO2 Compressor Operating in Near-Critical Conditions," in *The 7th international supercritical CO2 power cycle symposium*, San Antonio, Texas, 2022.

[25] K. Ringstad, Y. Allouche, P. Gullo, Å. Ervik, K. Banasiak and A. Hafner, "A detailed review on CO2 two-phase ejector flow modeling," *Thermal Science and Engineering Progress ,* 2020.

[26] S. D. Cich, J. Jeffrey Moore, M. Marshall, K. Hoopes, J. Mortzheim and D. Hofer, "Radial Inlet and Exit Design for a 10 MWe sCO2 Axial Turbine," in *ASME Turbo Expo 2019*, 2019.

[27] A. Hosangadi, Z. Liu, T. Weathers, V. Ahuja and J. Busby, "Modeling Multiphase Effects in CO2 Compressors at Subcritical Inlet Conditions," *Journal of Engineering for Gas Turbines and Power,* vol. 141, 2019.

DOI: 10.17185/duepublico/77332

DOI: 10.17185/duepublico/77332
URN: urn:nbn:de:hbz:465-20230427-152221-4